Available online at www.sciencedirect.com
SCIENCE DIRECT®
Journal of Hydrology 318 (2006) 262–275
Journal of Hydrology
www.elsevier.com/locate/jhydrol

Analytic element solutions for seepage towards topographic depressions

A.R. Kacimov*

Department of Soils, Water, and Agricultural Engineering, Sultan Qaboos University, P.O. Box 34, Al-Khod 123, Oman

Received 27 October 2004; revised 29 May 2005; accepted 2 June 2005

Abstract

Point and line singularities are superposed with incident unidirectional saturated and unsaturated flows. The resulting isobars of 3D Laplacian or advective dispersion equation fields model either seepage face dimples and rills on a tilted hillslope or an undulated top of the vadose zone above a stagnant water table. The reconstructed shapes of isobars are conchoidal, i.e. convex–concave. All flow characteristics (drawdowns, velocity and Kirchhoff potential distributions, dimple sizes) are calculated either explicitly or by elementary computer algebra routines.

Keywords: Groundwater; Moisture flow; Evaporation; Seepage erosion; Analytic solutions

1. Introduction

Natural eolian erosion of dune-type (hummocky) landscapes in geomorphology or human-induced alterations of the land surface (e.g. artificial dimples and ditches dug in agricultural practice, grading of hill terraces, or quarries excavated in mining industry) affect the invisible subsurface hydrological systems. Prior to these changes groundwater and moisture in the subsurface can often be viewed as balanced. Reshaping of the surface can initiate or speed up the movement of dormant soil water or can drastically change its unidirectional path under flat topography. Seepage can focus to fens (humid climates) or sabkhas (arid conditions). In the latter regime water does not spring up and only indirect evidences of seepage, e.g. precipitates, can be detected on the surface (Yechieli and Wood, 2002).

In some cases, this topographically intensified discharge can be beneficial to the flora as plant roots can intercept moisture that exudes through water table—atmosphere shortcuts. In other situations (detrimental to agriculture), exfiltration causes salty lakes (brackish water discharging directly to the surface) or patchy salt crust accumulation on undulation slopes (evaporative moisture fluxes). Deleterious consequences of focused seepage are well-known to geotechnical engineers as piping (Ojha et al., 2003). This relatively fast phenomenon, which is similar to a slower process of incision of valley landforms by groundwater (i.e. without any runoff erosion), is characterised by a 'finger' which evolves

* Tel.: +968 515 223; fax: +968 513 418.
E-mail addresses: anvar@squ.edu.om (A.R. Kacimov), anvar.kasimov@ksu.ru (A.R. Kacimov).

0022-1694/$ - see front matter © 2005 Elsevier Ltd All rights reserved.
doi:10.1016/j.jhydrol.2005.06.019

under a dam from the tail water to the upper pool. Seepage-induced channelization of tilted beaches dissected by periodically appearing short-lived rills (effaced by tide waves) is another example of essentially 3D pattern formation, analysed recently by Schorghofer et al. (2004). Positive feedback destabilizes the soil in piping and channelization because the hydraulic gradient in the proximity of 'fingers' amplifies with their growth and triggers ulterior metamorphosis of the topography (slumping and collapse of a soil massif).

In this paper, we present explicit analytic solutions to steady-state problems of saturated and unsaturated Darcian seepage near irregularities on an inclined and horizontal isobaric soil surface. For groundwater we consider the same flow pattern as in Schorghofer et al. (2004), i.e. a horizontal incident flow discharging through a tilted seepage face with a dimple that disturbs this 1D scenario. A genuinely 3D problem is obtained for an isobaric rill draining an incident flow streaming to a tilted seepage face. For unsaturated conditions we study spatial distortion of an incident 1D flow from/to a horizontal water table to/from the soil surface with a dimple serving as a locus of an axisymmetric converging flow. Explicit analytical solutions in terms of the hydraulic head or suction pressure distributions are obtained by the method of analytic elements (Strack, 2003). We tackle the same Rankine-type flow patterns and singularities as in Kacimov (2000a)—point sinks, sources and dipoles placed in a unidirectional flow.

2. Groundwater flow to a hillslope dimple

Based on our assumptions, in saturated conditions the hydraulic head $h(x, y, z)$, which is measured from the origin of coordinates O of a Cartesian system xyz (Oz—axis is counter-oriented with the vector of gravity $\vec{g}$), satisfies the Laplace equation. The velocity potential $\Phi = -kh$, where k is the soil conductivity, is also a harmonic function.

In congruity with Schorghofer et al. (2004) experiments, we study a porous wedge with a horizontal impermeable base $F_1F_4E_2E_1$ (Fig. 1a). A constant head vertical boundary $F_1F_2F_3F_4$ is distance L from the wedge edge and the groundwater level there is H above the base. The wedge angle is α and it extends infinitely in y-direction. The tilted plane $F_2F_3E_2E_1$ is isobaric, i.e. all water that seeps out either evaporates or runs off without any ponding. If $F_2F_3E_2E_1$ is smooth, then seepage is perfectly 1D with a horizontal specific discharge $v_s = kH/L = k \tan \alpha$ (Polubarinova-Kochina, 1977 abbreviated further as PK).

As Schorghofer et al. (2004) showed, a rill BC (Fig. 1b), which emerges due to local erosion, makes seepage 3D, i.e. this channel, topographically depressed with respect to $F_2F_3E_2E_1$, focuses groundwater flow. Schorghofer et al. (2004) assumed that the channel is empty and modeled numerically its bottom as a fixed seepage face boundary.

We shall not prescribe the shape of BC, as Schorghofer et al. (2004) did, but reconstruct it as a part of solution using the method that PK classified as semi-inverse. The method assumes that the flow domain boundary or its part is derived from a prescribed distribution of hydrodynamic singularities (or equivalently, from a postulated domain in one of characteristic planes—hodograph, Zhukovskii function, etc.). For example, a hydrodynamic source placed in a unidirectional flow generates a division boundary (which in what follows will be called a separatrix), which is considered as a semi-infinite impermeable body disturbing the ambient uniform flow (e.g. Panton, 1984). This idea dates back to Rankine who designed ship shapes by distributing different singularities in an incident flow. The method was well-accepted by groundwater hydrologists (PK). Kozeny channels, ultimately stable slopes and optimal hydraulic structure contours (PK, Kacimov, 2001; Kacimov and Obnosov, 2002) have been found by this method in saturated conditions. In soil physics the approach has been recently implemented for the Gardner soil (Warrick and Fennemore, 1995) when flow is governed by the advective dispersion equation (ADE).

The semi-inversely reconstructed shapes both in fluid and subsurface mechanics do not coincide with real ones. Topography, with already complex catchment-scale relief features, upon zooming in reveals intricate concave and convex zones interspersed by man-made berms, banquettes, opencast sites, furrows, etc. The analytic shapes, however, can be close to these elements of natural landforms or geotechnic objects. For instance, Fujii and Kacimov (1998)

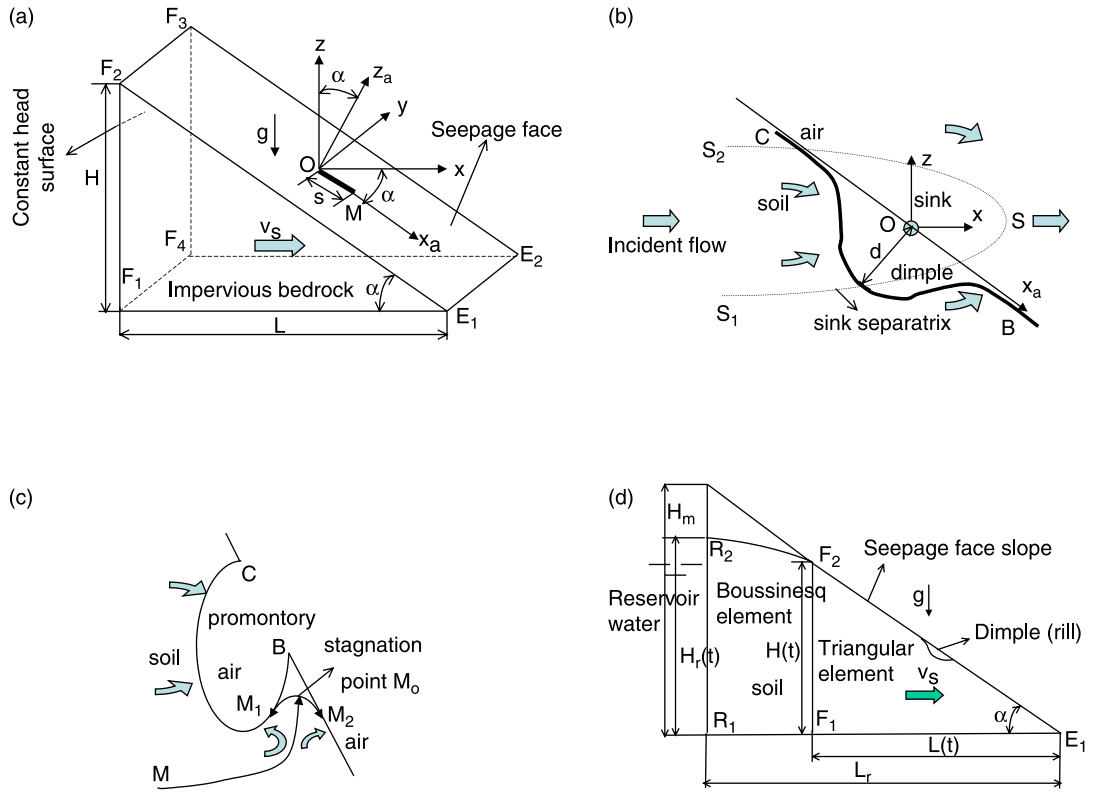

Fig. 1. Saturated wedge with horizontal seepage (a), vertical cross-section passing through the dimple axis (b), nontrivial micromound of groundwater (c), dam section with a transient phreatic surface (d).

calculated a sink-induced shape of an empty (isobaric) tunnel draining a ponded soil surface that at certain conditions is nearly circular while a filled (constant head) tunnel is always circular (PK). Since our governing equations—the Laplace and ADE—are elliptic the net effect of the derived shapes on the ambient pressure field is spatially limited. In other words, far enough from the placed singularities the disturbance introduced by them on the ambient field decays with asymptotics described by PK for the Laplace equation and by Philip et al. (1989) for ADE. In this sense the semi-inversely calculated forms might not be worse than regular shapes posited in the direct method (e.g. a putatively rectangular rill of Schorghofer et al., 2004), which also, only attempt to mimic the 'real' geometry.

The simplest analytic elements that we combine in order to simulate seepage near a dimple in Fig. 1b is a unidirectional flow and a sink at point O (PK) such that the resulting potential is:

$$\Phi(x,y,z) = k\tan\alpha x + \frac{q}{4\pi\sqrt{x^2+y^2+z^2}} \tag{1}$$

where q is the strength of the superposed sink. Now, we search for a surface BC which satisfies the seepage face condition $\Phi + kz = 0$, i.e. using (1) and this seepage face condition we get the equation

$$x\tan\alpha + z = -\frac{q}{4k\pi\sqrt{x^2+y^2+z^2}} \tag{2}$$

We transform our coordinate system as

$$\begin{aligned} x &= x_a\cos\alpha + z_a\sin\alpha, \qquad y_a = y, \\ z &= -x_a\sin\alpha + z_a\cos\alpha \end{aligned} \tag{3}$$

i.e. align the Ox_a axis with the slope surface, and the Oz_a axis normal to it.

Using (3) we simplify (2) to a quartic whence the final equation of our *BC* follows

$$z_a = -\sqrt{\frac{\sqrt{\rho_a^4 + 4a^2} - \rho_a^2}{2}}, \qquad a = \frac{q\cos\alpha}{4\pi k}, \qquad \rho_a = \sqrt{x_a^2 + y_a^2} \tag{4}$$

As is clear from (4), in the system $x_a y_a z_a$ the dimple is axisymmetric, i.e. its shape is the same in any plane passing through Oz_a line. The dimple depth measured along Oz_a is $d_a = \sqrt{a}$. The asymptotics of the crater banks is $\rho_a \sim -1/z_a$ as $z_a \to -0$. We select dimensionless coordinates as $(X, Y, Z, R) = (x_a, y_a, z_a, \rho_a)/\sqrt{a}$. Fig. 2 shows the dimple contour (one half due to symmetry) in a cross-section perpendicular to the plain *XOY* and passing through point *O*. The inflexion point of this curve is $R_i = (4/3)^{1/4} \approx 1.075$, $Z_i = -1/3^{1/4} \approx -0.76$. The contour equation in polar coordinates is $\vec{\rho}_p = 1/\sin\omega$ where ω is the angle measured from the plane *XOZ* to the contour point and $\vec{\rho}_p$ is the contour point radius vector originated at *O*. This curve belongs to the class of conchoids, which were recently shown to possess amazing optimality features (Kacimov, submitted).

The Stokes stream function Ψ, which corresponds to the field (1), can be found elsewhere (e.g. Panton, 1984). For the plane $y = 0$ it is

$$\Psi = 0.5k\tan\alpha\, z^2 - \frac{q}{4\pi}\left(1 + \frac{x}{x^2 + z^2}\right)$$

$$V_{BC} = \sqrt{\tan^2\alpha + \frac{4}{\cos^2\alpha(R^2 + R_4)^2} - 4\frac{\sqrt{2}x\tan\alpha - \sqrt{R_4 - R^2\tan^2\alpha}}{(R^2 + R_4)^{3/2}}} \tag{5}$$

We plotted streamlines Ψ/q in Fig. 3 with the dimple contour shown in bold for $q = 1$ and $\alpha = \pi/4$.

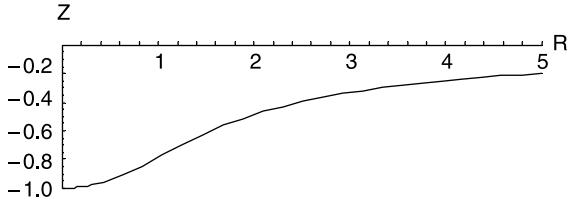

Fig. 2. Contour of a sink-induced dimple (SID).

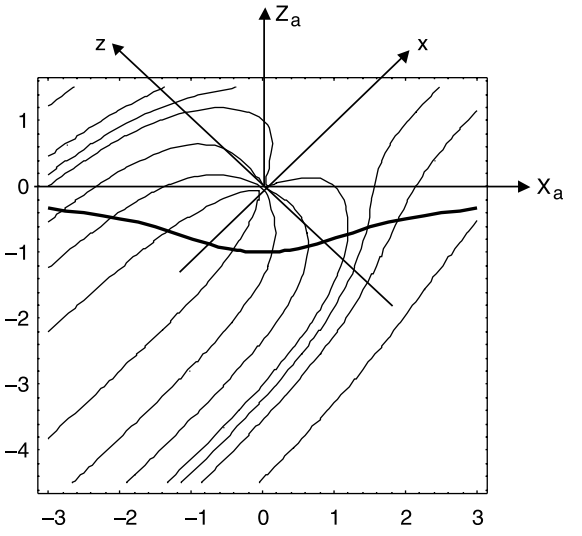

Fig. 3. Streamlines in an axial section $y = 0$ of SID, $q = 1$, $\alpha = \pi/4$.

Clearly, everything that is above the contour in Fig. 3 is not physical (air zone) and should be truncated. In xOz plane (Fig. 1b) the dashed line is the Rankine body contour, which we define as a streamline defined as separatrix S_1SS_2. In groundwater hydrology, this separatrix demarcates the part of an incident groundwater flow intercepted by a well (Kinzelbach et al., 1992).

From (1) we calculate the magnitude of the specific discharge vector as $|\vec{v}| = \sqrt{\Phi_x^2 + \Phi_y^2 + \Phi_z^2}$. Along *BC* we come after some algebra to:

where $R_4 = \sqrt{R^4 + 4}$ and $V = |v|/k$.

Fig. 4a shows $V(X)$ at $Y = 0$ and $\alpha = \pi/3$, $\pi/4$, $\pi/8$ (curves 1–3, correspondingly) calculated from (5). Fig. 4b shows $V(X)$ at $Y = 1$ for the same values of α. According to (5) and the graphs $V \to \tan\alpha$ at $X \to \pm\infty$, but the velocity limit is reached from above for the uphill part of the transects and from below—for the downhill ray. There is a maximum and minimum for each $V(X)$ curve in Fig. 4. These extrema become more pronounced with the increase of α and with approaching the plane $Y = 0$.

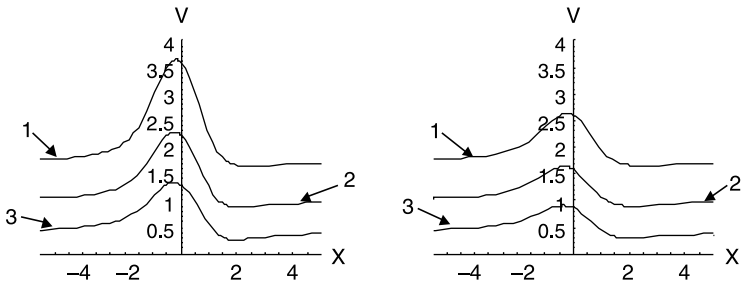

Fig. 4. Magnitude of velocity along the SID contour in cross-sections $Y=0$ (a) and $Y=1$ (b), curves 1–3 correspond to $\alpha=\pi/3$, $\pi/4$, $\pi/8$.

For stability of the dimple, the most important parameter is the peak V_{max} and the location X_{max} of this maximum, which are shown in Fig. 5 (curves 1 and 2) as functions of α at $Y=0$. The extrema in Fig. 5 and below were found by the FindMinimum routine of *Mathematica* (Wolfram, 1991). Fig. 5 shows that V_{max} far exceeds the critical value, which PK determined to be 1 for cohesionless soils. It might explain why small depressions in Schorghofer et al. (2004) experiments evolve in long rills.

We note that the local slope angle is also important to assess the seepage-induced instability because high V at the spot of the dimple normal to $\vec{g}$ will only cause hovering ('boiling') of dismembered soil particles while on steeper parts of the slope gravitational sliding can also occur (Kacimov and Obnosov, 2002).

The velocity minimum V_{min} and its locus X_{min} are shown in Fig. 6 as functions of α at $Y=0$. Curiously enough, that for a specified rill shape, along with a trivial phreatic surface shown in Schorghofer et al. (2004), a phreatic surface $M_1M_0M_2$ can form near the promontory B in Fig. 1c similarly to PK (Fig. 157). At stagnation point M_0 the streamline of groundwater flow bifurcates, i.e. a micromound is formed. Water moves from the separatrix MM_0 to two different vents (alcove and slope). The area $BM_1M_2M_0$ lies above the micromound but can be madefied by capillarity. In our semi-inverse model and flow scheme phreatic surfaces do not exist but a zone of relatively small groundwater velocity can be detected by V_{min}.

Fig. 7 presents the graphs $V(Y)$ at $\alpha=\pi/4$ and $X=-1$, 0, 2 (curves 1–3). The graphs show that in these sections the dimple can both increase and decrease the velocity with respect to the background flow.

We recall that the influence of a point sink is proportional to $1/r$ where r is the distance to the sink. Consequently, point O in Fig. 1a should be far enough from $F_1F_4E_2E_1$ to neglect this influence and to neglect the fact that a single sink perturbs the no-flow condition along the base. This can be rectified by an

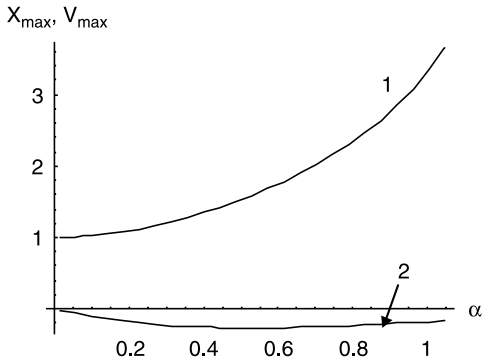

Fig. 5. Global maximum V_{max} of velocity (curve 1) on the SID contour and its abscissa X_{max} (curve 2) as functions of slope.

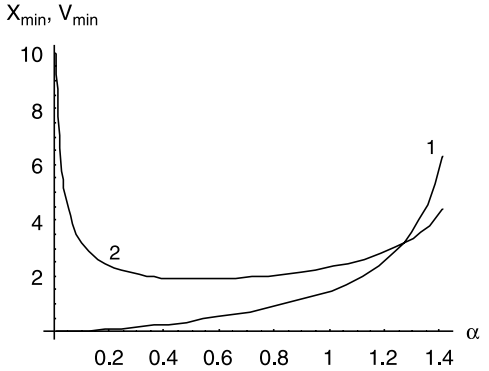

Fig. 6. Global minimum of velocity V_{min} (curve 1) on the SID contour and its abscissa X_{min} (curve 2) as functions of slope.

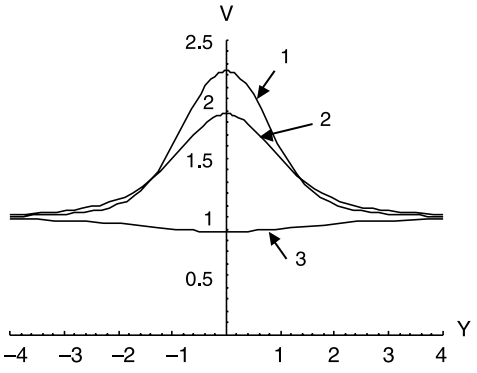

Fig. 7. Magnitude of velocity along the SID contour in cross-sections $X=-1$, 0, 2.

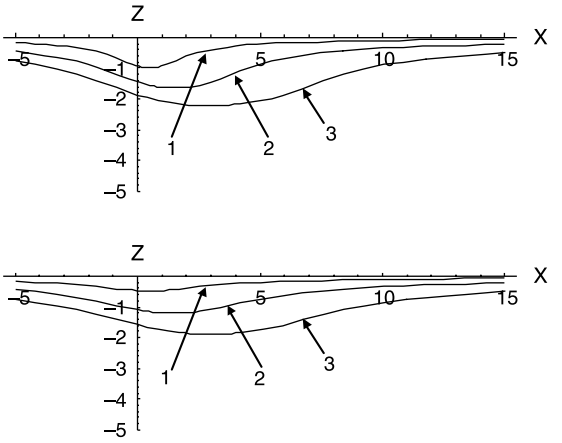

Fig. 8. Rill contours for different lengths of inducing line sinks, cross-sections $Y=0$ and 1, curves 1–3 correspond to $S=1$, 3, 6.

image source under $F_1F_4E_2E_1$ that will be illustrated in Section 4.

3. Flow to a rill

In order to model Schorghofer et al. (2004) channels, i.e. depressions elongated in the x_a direction, we use another analytic element, a linear sink (well). In all other sections of the paper problems are axisymmetrical with respect to the vertical axis while in this section the arbitrary orientation of the sink makes the problem genuinely 3D. In this case the Stokes scalar stream function is not applicable and one should deal with a vector potential as a stream function (Steward, 2002).

We assume that along a rectilinear segment OM of a length s (Fig. 1a) sinks are distributed uniformly with a constant strength q_s per unit length such that the total strength of the element is sq_s. In other words, we place a well of an infinitesimal radius just on the slope surface. PK gave the corresponding potential as

$$\Phi_w = \frac{q_s}{4\pi}\log\frac{s-x_a+\sqrt{(s-x_a)^2+y_a^2+z_a^2}}{\sqrt{x_a^2+y_a^2+z_a^2}-x_a} \tag{6}$$

Combining (6) with the incident unidirectional flow (1) and searching for a seepage face boundary $\Phi+kz=0$ we arrive at an equation of the rill surface

$$Z = \log\frac{S-X+\sqrt{(S-X)^2+Y^2+Z^2}}{\sqrt{X^2+Y^2+Z^2}-X}, \qquad a = \frac{q_s\cos\alpha}{4\pi k} \tag{7}$$

where $(X, Y, Z, S)=(x_a, y_a, z_a, s)/a$, i.e. Z is dimensionless deviation of the rill surface from the slope plain. Unlike the dimple, we could not solve (7) explicitly and FindRoot of *Mathematica* was used. In this way we present in Fig. 8 the contours $Z(X)$ for $S=1$, 3, 6 (curves 1–3) in cross-sections $Y=0$ and $Y=1$ (upper and lower graphs) in Fig. 8. Contours $Z(Y)$ in cross-sections $X=-2$, 0, 2 (from left to right) are shown in Fig. 9. We skip over the analysis of the rill velocity field.

We note that the Schorghofer et al. (2004) apparatus with a constant head H in Fig. 1a can be viewed as an analytic element of a transient background system with a reservoir water level $H_r(t)$ (Fig. 1d) varying with time. Then at $H_r(t)<H_m$ a free surface F_2R_2 is formed. If H_r is monotonic as for example in Kacimov and Yakimov (2001) then the height $H(t)$ of the Schorghofer et al. (2004) triangular element at each instant can be approximated by the Pavlovskii (PK) formula

$$H(t) = \frac{H_r^2(t)}{\tan\alpha\left(L_r+\sqrt{L_r^2-H_r^2(t)\tan^{-2}\alpha}\right)} \tag{8}$$

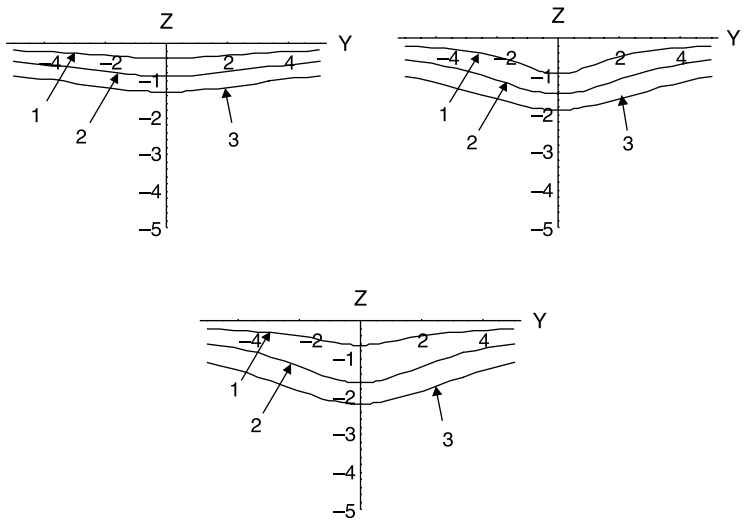

Fig. 9. Rill contours for different lengths of inducing line sinks, cross-sections $X=-2$, 0, 1 (from left to right).

which is based on the Dupuit–Forchheimer approximation and which, as PK proved for steady regimes, matches with the full potential solution. If our emerged dimple or rill is downstream of the constant head section F_2F_1 (but still well above R_1E_1), then we can model seepage towards it as steady state. Indeed, the recession of $H_r(t)$ (as in Schorghofer et al., 2004, field conditions) causes a drop of R_2F_2 and a change of $E_1F_1F_2$ ensues. The velocity $v_s=kH(t)/L(t)$ remains, however, constant (of course, if the Boussinesq equation in the element $R_1R_2F_2F_1$ holds).

We stress that by (6) the 'gaining' nature of the rill is postulated. However, any surface channel (well, river, lake, etc.) can also be 'losing' or of a 'flow-through' type (Kacimov, 2000a, Steward and Jin, 2001). Fissiparous or coupling rills can be easily modeled by three line sinks crossing at one point. The whole rill pattern is a composition of multiple line sinks.

4. Dimple draining a phreatic surface flow

In the previous two sections the undisturbed flow was horizontal and generic to the so-called dam problem of PK. Few modifications are necessary to convert our solutions to a free surface flow over a tilted impervious layer.

As balanced conditions we consider a uniform groundwater flow over an impermeable bedrock $E_1F_1F_4E_4$ that dips at an angle α (Fig. 10a). The water table $E_2F_2F_3F_3$ is a perfect plane, which is parallel to the bed and the saturated thickness is H. The velocity magnitude of this uniform flow is $v_s=k\sin\alpha$.

According to PK, flow in Fig. 10a can originate from a feeding reservoir in the uphill part as depicted in Fig. 10b, which represents a longitudinal cross-section of the flow domain in Fig. 10a. The reservoir bottom is sloped at an angle $\pi/2-\alpha$, the free boundary is exactly a ray Ux_a perpendicular to the reservoir bottom and the flow domain is a quadrant. Because all streamlines are straight and parallel to the free surface we can select any of them as an impermeable bed. Note, that both the Dupuit–Forchheimer approximation and the full potential theory give identical flows for the regime in Fig. 10b (PK).

Thus the background (pre-dimple) potential is $\Phi_u=kx\sin\alpha\cos\alpha-kz\sin^2\alpha$. We combine it with a point sink potential and search for an isobaric dimple contour. Rotating the axes according to (3), i.e. aligning Ox_a with the undisturbed free-surface, the isobar $\Phi+kz=0$ is obtained from the equation

$$z_a=-\frac{q}{4\pi k\cos\alpha\sqrt{x_a^2+y_a^2+z_a^2}}, \tag{9}$$

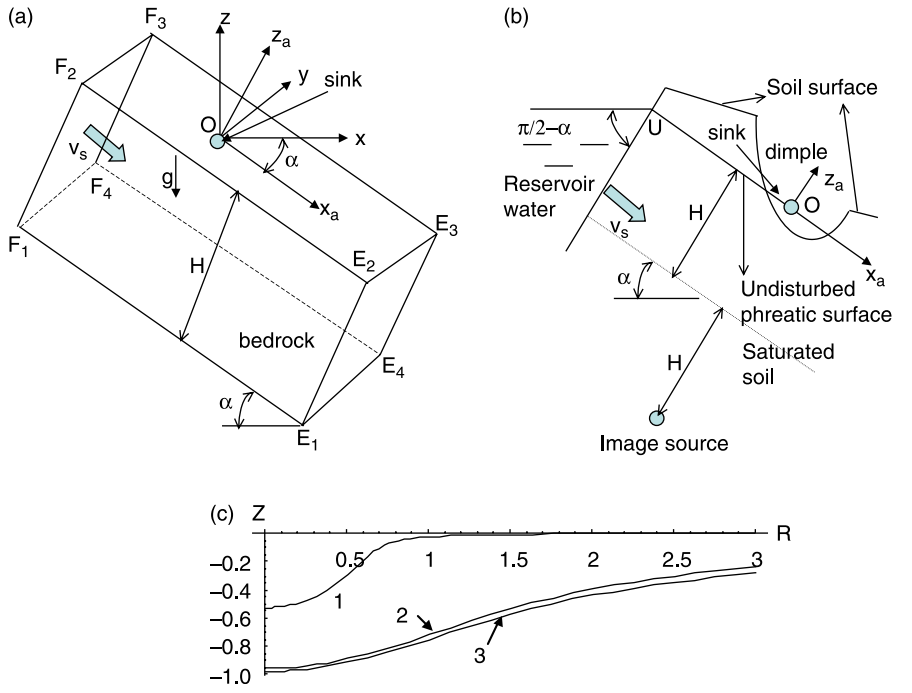

Fig. 10. SID in a phreatic surface flow over a dipping bed; 3D view (a), a vertical cross-section (b), rill contours for dimensionless base depths $D=0.1$, 5, 10 (curves 1–3).

Evidently, (9) is reduced to (4). The only difference with (4) is that now $a=a_f=q/(4\pi k\cos\alpha)$. Therefore, the dimple shape coincides with that one shown in Fig. 2 (coordinates normalised to the new value of $\sqrt{a_f}$).

If we use a single sink, then its action does not preserve the no-flow condition along $E_1F_1F_4E_4$ and $E_2F_2F_3F_3$ (recall that the isobaricity condition along the dimple contour is rigorously satisfied in the semi-inverse method). This may be quite important as flows over sloping beds often are shallow, i.e. H in Fig. 10 can be small. Consequently, now we shall add an image source placed at point $x_a=0$, $y_a=0$, $z_a=-2H$. Then the sink–source pair provides the no-flow condition along $E_1F_1F_4E_4$ in Fig. 10a. Obviously, the image source will affect less the area $F_2F_3E_3E_2$ than the sink.

We introduce dimensionless coordinates $(X,Y,Z,R,D)=(x_a,y_a,z_a,\rho_a,H)/\sqrt{a_f}$. Then the contour of a sink–source generated atmospheric pressure isobar is searched as a solution of the 12-th order algebraic equation with respect to Z, which follows from

$$Z=-\frac{1}{\sqrt{R^2+Z^2}}+\frac{1}{\sqrt{R^2+(Z-2D)^2}} \tag{10}$$

Again, we used the FindRoot routine of *Mathematica* to determine the roots of (10). Fig. 10c shows the calculated half-contours for $D=0.1$, 5, 10 (curves 1–3, correspondingly). Curves 2 and 3 practically coincide, that implies that we can assume $D=\infty$ i.e. instead of an implicit solution of (10) we can use the explicit conchoid Eq. (4) (remember the change $a\to a_f$).

5. Moisture flow to a dimple

Evaporation/infiltration through the soil surface is usually (Philip, 1991) modeled under the assumption of its flat topography. A flat water table beneath makes the problem 1D. However, both boundaries can be tilted or curved that calls for 2D or 3D analysis (Kacimov, 2003, 2004, Kacimov et al., 2004).

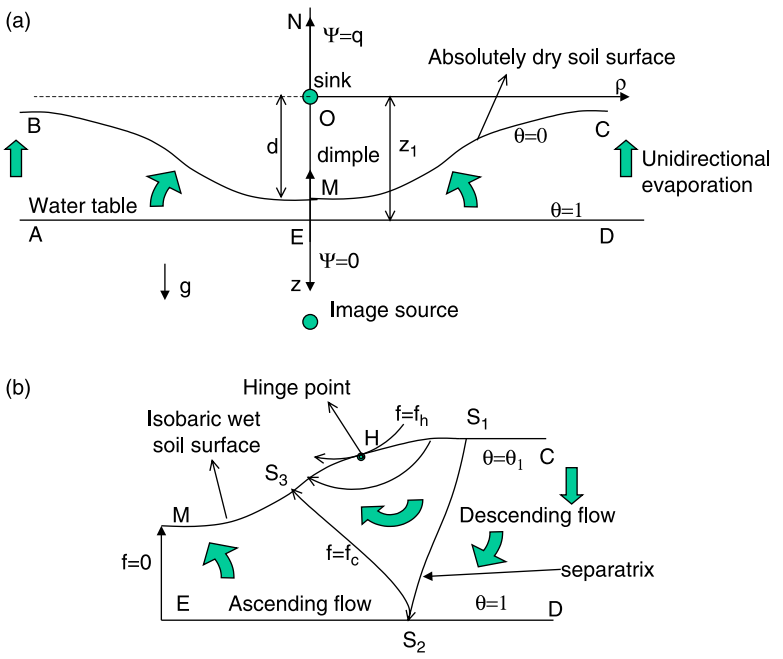

Fig. 11. Vertical (axial) cross-section of SID in the vadose zone; evaporating (a) and flow-through (b) dimple.

In this section we consider axisymmetric unsaturated exfiltration-infiltration from a horizontal water table *AED* towards a dimple *BMC* that is maintained at constant suction (Fig. 11a illustrates a vertical cross-section). Far from *Oz* the soil surface is horizontal and coincides with the *xOy* plane of a Cartesian coordinate system *xyz*, with the *z*-axis co-oriented with $\vec{g}$. The asymptotic thickness of the horizontal layer is z_1. Therefore, at large $\rho = \sqrt{x^2+y^2}$ flow is purely vertical, i.e. we have infiltration to the water table at high moisture content of the soil surface and exfiltration (evaporation) from the water table if the soil surface is dry enough. At small ρ a preferential moisture flow is funneled to *BC*.

We recur to the quasilinear model and for the sake of brevity drop the model description referring the reader to Philip (1989). We shall use all notations from Philip's Eq. (1) to Eq. (8). The dimensionless Kirchhoff potential θ satisfies the ADE in cylindrical coordinates:

$$\frac{\partial^2\theta}{\partial\rho^2}+\frac{\partial^2\theta}{\partial z^2}+\frac{1}{\rho}\frac{\partial\theta}{\partial\rho}-2\frac{\partial\theta}{\partial z}=0 \tag{11}$$

Philip (1989) considered the case of infiltration from a point source set above the water table. He combined the Kirchhoff potential of this source with an image sink located symmetrically under the water table and with an ambient stagnant moisture distribution in an upper half-plane. Philip derived an explicit solution in terms of the potential for the domain above the water table. The vicinity of the Philip source is to be excluded from the solution domain as the Kirchhoff potential there exceeds the saturation limit and the quasilinear model breaks.

In our application we invert the Philip solution, i.e. we put a sink above the water table and an image source below the water table (Fig. 11a). Besides, we generalise the ambient conditions at large ρ, as we did in Kacimov (2000b) with another flow pattern of Philip, i.e. we consider a uniform flow to/from a flat soil surface.

Thus, according to Philip (1989) the sink–source pair mirrored about the water table generates the Kirchhoff potential

$$\theta_{ss}=-\frac{Q\exp z}{8\pi}\left[\frac{\exp(-r)}{r}-\frac{\exp(-r_1)}{r_1}\right],\qquad r=\sqrt{\rho^2+z^2},\quad r_1=\sqrt{\rho^2+(z-2z_1)^2} \tag{12}$$

where $Q>0$ is a dimensionless strength of each singularity.

If a horizontal soil surface (Fig. 11a, dashed line) were maintained at potential θ_1 then the corresponding potential there would be

$$\theta_v = \theta_1 + (1-\theta_1)\frac{\exp(2z)-1}{\exp(2z_1)-1} \tag{13}$$

As we can readily infer from (13), background evaporation occurs at $\theta_1<\exp(-2z_1)$; at $\theta_1>\exp(-2z_1)$ we have descending infiltration and $\theta_1=\exp(-2z_1)$ corresponds to the Philip (1989) regime of a stagnant ambient moisture.

By summing (12) and (13) we get the full potential as

$$\theta = \theta_{ss} + \theta_v \tag{14}$$

The Stokes stream function f (defined by Philip, 1989, Eq. 12) satisfies the equation

$$\frac{\partial^2 f}{\partial \rho^2} + \frac{\partial^2 f}{\partial z^2} - \frac{1}{\rho}\frac{\partial f}{\partial \rho} - 2\frac{\partial f}{\partial z} = 0 \tag{15}$$

For our sink–source pair this function (metaharmonically conjugated with the potential component (12) and satisfying (15) in the sense of Bystrov, 1959) is expressed as:

$$f_{ss} = 1 - \frac{\exp z}{2} \times \left[\frac{(r+z)\exp(-r)}{r} - \frac{(r_1+z-2z_1)\exp(-r_1)}{r_1}\right]. \tag{16}$$

We emphasize that in (16) $f_{ss}=1-f_1$ where f_1 is the corresponding Philip's (1989) function, Eq. (16). This difference is due to inversion of Philip's singularities i.e. we set $f_{ss}=0$ along the segment OM and $f_{ss}=1$ along the ray ON while Philip's pair has $f_1=-1, 0$, respectively.

The stream function that corresponds to the background exfiltration-infiltration potential (13) is

$$f_v = \frac{4\pi}{Q}\frac{1-\theta_1\exp(2z_1)}{\exp(2z_1)-1}\rho^2 \tag{17}$$

and the linearity of the quasilinear model allows us to assemble the full stream function:

$$f = f_{ss} + f_v \tag{18}$$

Fig. 12a portrays the right half of isobaric lines, $\theta=$const and stream lines; $f=$const plotted in coordinates $(\rho, -z)$ by ContourPlot of *Mathematica* for $Q=1$, $z_1=1$, $\theta_1=0$ (isopotential lines spanning from $\theta=0$ to 0.8 with an increment of 0.2 and streamlines $f=0.5, 2.5, 5.5, 10.5, 15.5$). The upper curve indicates the dimple contour $\theta=0$. As usually in the semi-inverse technique, the part of the flow domain above BC should be discarded.

Fig. 12b illustrates the flow net for $\theta_1=0.14$ and the same Q and z_1 as in Fig. 12a with equipotential lines $\theta=0.14, 0.2, 0.4, 0.6, 0.8$ and streamlines $f=0.2, 0.4, 0.6, 0.613, 0.753$. The isopotential lines are qualitatively the same as in Fig. 12a but the streamlines are not. The first peculiarity of the isobaric dimple in Fig. 12b is the existence of a critical streamline $f_c=0.613$, which divides the soil into three subdomains. This separatrix is shown schematically in Fig. 11b as $S_1S_2S_3$. In Fig. 12b, it is the only nonsmooth streamline that is kinked at point S_2 where the flux vector swerves (compare with kinked streamlines in PK and Kacimov and Youngs, 2005). At this (and only this) stagnation point (remember that we work in an axial cross-section, i.e. S_2 is a trace of a 3D stagnation circle) all three forces—gravitational, capillary, viscous resistance coined in terms of the Darcy law—which govern the movement of moisture are balanced.

To the right of $S_1S_2S_3$ moisture moves from the soil surface to groundwater and f decreases there from f_c to $-\infty$ (recall that Philip's, 1989 stream function was limited as $0<f_1<1$). Between ME and S_2S_3 water table loses moisture to the dimple and $0<f<f_c$. Above $S_1S_2S_3$ we have $f_c<f<f_h$, moisture makes a loop, i.e. it infiltrates to the subsurface from S_1H and exfiltrates through HS_3 where H is a hinge point similar to the Toth model of topographically driven groundwater (Kacimov, 1996).

For our example the line $f_h=0.753$ marks the hinge point by just touching the dimple contour. Within the flow domain in our porous layer f_h gives an absolute maximum of f although in the truncated air part above MHS the stream function increases further. Because f increases from 0 to f_h along MH the maximum f_h corresponds to the total amount of exfiltration through the soil surface (we recall that in congruity with our normalization $f_{OM}=0$ the Stokes stream function at certain ρ equals the total flow rate through a circle of

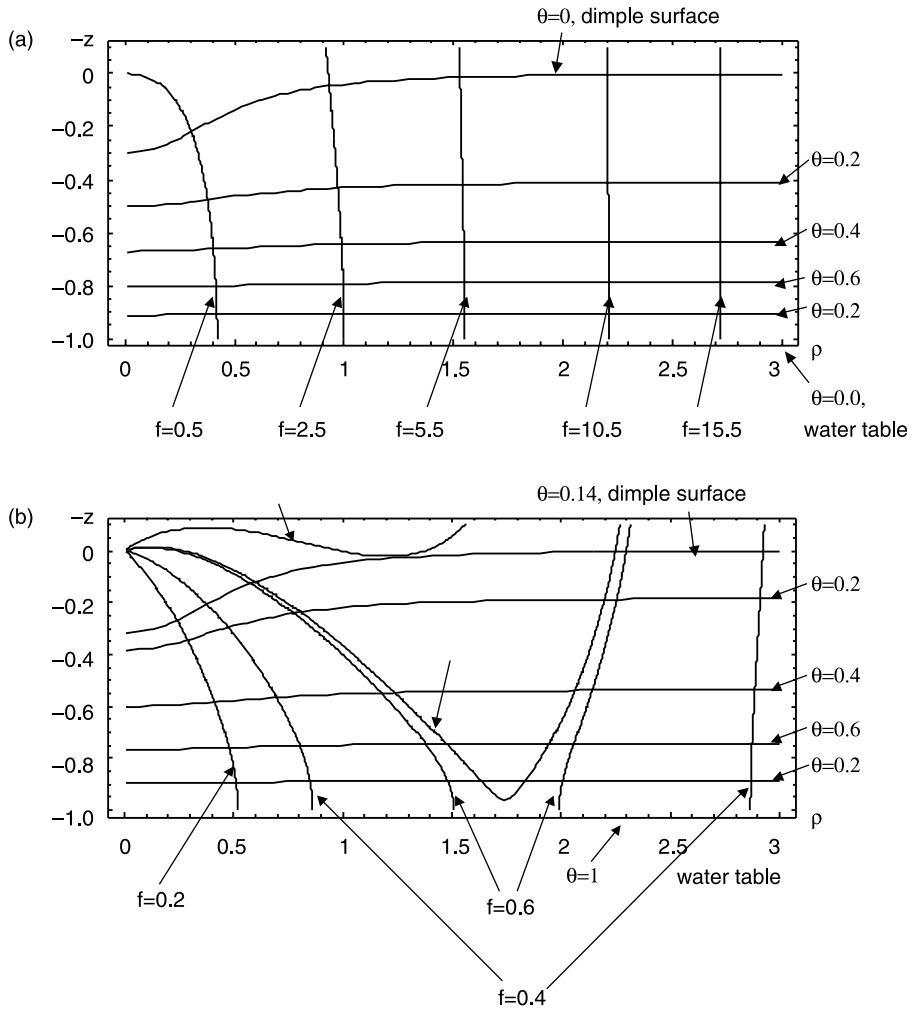

Fig. 12. Flow net for a quasilinear SID at $Q=1$, $z_1=1$; soil surface under infinite tension (a) and relatively wet surface (b).

radius ρ). A part f_c exudes through MS_3 as originated from the water table. The rest (f_h-f_c) oozes out through S_3H and enters the soil through HS_1. The subsurface residence time of this part of our flow that circulates around H is small and the quality of this water is different as compared with what ascends from the water table. We can call the near-H zone a fast return flow (we recall that either rain or irrigation should madefy continuously BMC in order to maintain this circulation). The stream lines $f=0.2$, 0.4, 0.6 in Fig. 12a are disconnected within our soil layer, i.e. they consist of two branches each.

The vertical, v_z, and radial v_ρ components of velocity (Philip's Eq. (12)) were also expressed explicitly by direct differentiation of (14) or (18) with the help of a build-in function D of *Mathematica* (we drop these formulae here). In Fig. 13, we show $v_z(\rho)$ at $z=1$, $Q=1$, $z_1=1$ for $\theta_1=0.12$, $\exp[-2]\approx 0.135$, 0.14, 0.204, 0.3 (curves 1–5). Curve 1 illustrates the case of a sufficiently dry soil (pure exfiltration). Curve 2 corresponds to the critical limit when outside the dimple moisture is stagnant. Curve 3 intersects the abscissa axis (that corresponds to point S_2 in Fig. 11b). Curve 4 represents the limiting case when point S_2 in Fig. 11b merges with point E. Curve 5 shows the case of pure infiltration. There is a remarkable analogy between the flow topology in Fig. 11 and losing–gaining sections of constant head

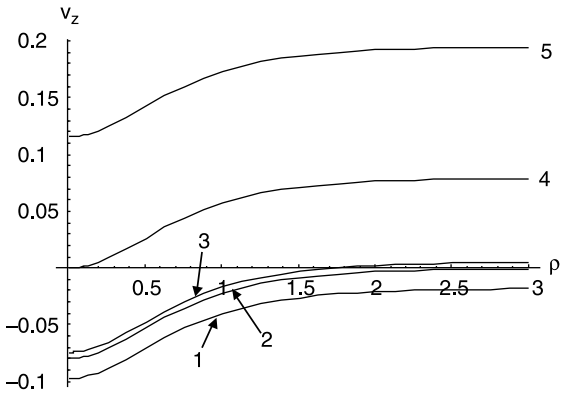

Fig. 13. Vertical component of velocity along the water table at $z=1$, $Q=1$, $z_1=1$ for $\theta_1=0.12$, $\exp[-2]\approx 0.135$, 0.14, 0.204, 0.3 (curves 1–5).

horizons in fully saturated artesian aquifers (Kacimov and Youngs, 2005).

The dimple depth $d=z_M$ is plotted in Fig. 14a as a function of z_1 at $\theta_1=0.14$ and $Q=0.1$, 0.5, 2.5 (curves 1–3). Fig. 14b shows d(Q) at $\theta_1=0.14$ and $z_1=1$, 2, 3 (curves 1–3).

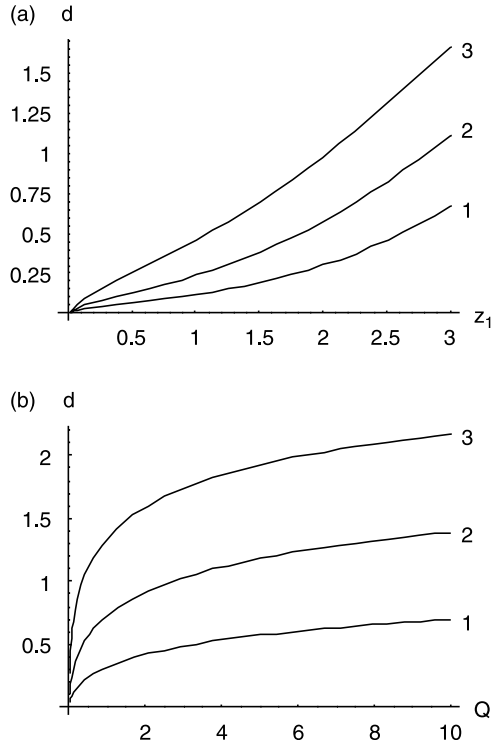

Fig. 14. Unsaturated SID depth for $\theta_1=0.14$ as a function of the asymptotic thickness of the soil layer at $Q=0.1$, 0.5, 2.5 (curves 1–3) (a) and of the sink strength (b) at $z_1=1$, 2, 3 (curves 1–3).

All the analysis above can be replicated for the Philip (1989) flow pattern with a source above the water table to which the potential (13) is added. Then the resulting semi-inverse isobar will model a topographical hump, whose apex zone, possessing a higher total head, will generate a return flow to a planar lowland.

We note that the horizon AD in Fig. 11 can be substituted by a more adequate trough-shaped water table (Kacimov and Youngs, 2005) from which water is lost for nonuniform evaporation. The water table depression can be modeled as another reconstructed equipotential $\theta=1$ of our contiguous sink and source with the latter having smaller strength than the former. The groove on the water table will be proportional to the disbalance of the singularities.

6. Conclusion

By the method of analytic elements we obtained rigorous solutions to problems of axisymmetric and 3D seepage when a flat or tilted soil surface is topographically disturbed by a dimple or rill that act as shortcuts for saturated or unsaturated seepage. In its standard form the method is implemented through distribution of singularities and determining their intensity from the condition of a given shape of an object (an airfoil, condenser, lake, soil heterogeneity, etc.) placed in a background flow (Bakker and Nieber, 2004; Lifanov, 1995; Strack, 2003). We followed a semi-inverse approach of PK and, in lieu of specifying the boundaries of the flow domain, we reconstructed its part—a dimple or rill—as an isobaric surface mathematically emerging from superposition of singularities.

A sink-generated dimple contour satisfying a seepage face boundary condition is found in an explicit form for an incident horizontal groundwater flow discharging through a slope of arbitrary declivity. Slight modifications bring about exactly the same shape when the background flow forms a tilted phreatic surface parallel to a tilted base of a hillslope. The shape of a rill we reconstructed as a seepage-face isobar generated by a line sink interfering with an ambient uniform flow.

In furtherance of Philip's (1989, 1991) quasilinear solutions for the vadose zone flows we placed a point source and sink in such a manner that the flow domain had a horizontal isobaric surface (water table) and a dimpled isobaric shape above the water table (undulated soil surface under constant suction). The sink deflects descending/ascending moisture flux and enables modeling evaporation and gravitational vent of moisture to a valley from a commanding plateau. As in the Toth model for saturated flows in hummocky landforms, the isobaric dimple slope has a varying total head that signifies intermittent zones of recharge and discharge.

The found convex–concave shapes and corresponding simple solutions can serve: as benchmarks for numerical codes; for assessment of tide-induced piping in the beach hyporheic zone; in estimates of intensification of flows to catchment-scale depressions, and thereby indication of the potential for erosion initiation and promotion of further erosion to make new landscape forms; in tuning-up standard evaporation models on the scale of catchments by taking into account relief features and intricate moisture circulation topology; etc.

Acknowledgements

This work was supported by project CL/SQU-UAEU/0/3/02. Materials on sabkha hydrology sent by W. Wood are appreciated. Criticism by two anonymous reviewers is appreciated.

References

Bakker, M., Nieber, J.L., 2004. Analytic element modeling of cylindrical drains and cylindrical inhomogeneities in steady two-dimensional unsaturated flow. Vadose Zone Journal 3, 1038–1049.

Bystrov, K.N., 1959. On two-dimensional steady flows in a layer with exponentially varying thickness. Transactions of the Moscow District Pedagogical Institute 75, 31–59 (in Russian).

Fujii, N., Kacimov, A.R., 1998. Analytic formulae for rate of seepage flow into drains and cavities. International Journal for Numerical and Analytical Methods in Geomechanics 22, 277–301.

Kacimov, A.R., 1996. Explicit solutions for seepage infiltrating into a porous earth dam due to precipitation. International Journal for Numerical and Analytical Methods in Geomechanics. 20, 715–723.

Kacimov, A.R., 2000a. Three-dimensional groundwater flow to a lake: an explicit analytical solution. Journal of Hydrology 240, 80–89.

Kacimov, A.R., 2000b. Circular isobaric cavity in descending unsaturated flow. Journal of Irrigation and Drainage, ASCE 126, 172–178.

Kacimov, A.R., 2001. Optimal shape of a variable condenser. Proceedings Royal Society London A 457 (N 2006), 485–494.

Kacimov, A.R., 2003. Unsaturated quasi-linear flow analysis in V-shaped domains. Journal of Hydrology 279, 70–82.

Kacimov, A.R., 2004. Capillary fringe and unsaturated flow in a reservoir porous bank. Journal of Irrigation and Drainage, ASCE 130, 403–409.

Kacimov A.R. Seepage to a drainage ditch and optimization of its shape. Journal of Irrigation and Drainage ASCE (submitted).

Kacimov, A.R., Yakimov, N.D., 2001. Moving phreatic surface in a porous slab: an analytical solution. Journal of Engineering Mathematics 40, 399–411.

Kacimov, A.R., Obnosov, Yu.V., 2002. Analytical determination of seeping soil slopes of a constant exit gradient. Zeitschrift fur angewandte Mathematik und Mechanik. 82, 363–376.

Kacimov, A.R., Youngs, E.G., 2005. Steady-state water-table depressions caused by evaporation in lands overlying a water-bearing substratum. Journal of Hydrological Engineering ASCE 10, 295–301.

Kacimov, A.R., Obnosov, Yu.V., Perret, J., 2004. Phreatic surface from a near-reservoir saturated tongue. Journal of Hydrology 296, 271–281.

Kinzelbach, W., Marburger, M., Chiang, W.H., 1992. Determination of groundwater catchment areas in 2 and 3 spatial dimensions. Journal of Hydrology 134, 221–246.

Lifanov, I.K. 1995. Methods of singular integral equations and numerical experiment. Moscow, Yanus (in Russian) (Engl. analogue: Lifanov, I.K. 1996. Singular integral equations and discrete vortices. Brill Academic Pub).

Ojha, C.S.P., Singh, V.P., Adrian, D.D., 2003. Determination of critical head in soil piping. Journal of Hydraulic Engineering, ASCE 129, 511–518.

Panton, R.L., 1984. Incompressible flow. Wiley, New York.

Philip, J.R., 1989. Multidimensional steady infiltration to a water-table. Water Resources Research 25, 109–116.

Philip, J.R., 1991. Upper bounds on evaporation losses from buried sources. Soil Sci. Soc. Amer. J. 55, 1516–1520.

Philip, J.R., Knight, J.H., Waechter, R.T., 1989. Unsaturated seepage and subterranean holes: conspectus, and exclusion problem for circular cylindrical cavities. Water Resources Research 25, 16–28.

Polubarinova-Kochina, P.Ya., 1977. Theory of Ground-water Movement. Nauka, Moscow (in Russian).

Schorghofer, N., Jensen, B., Kudrolli, A., Rothman, D., 2004. Spontaneous channelization in permeable ground: theory, experiment and observation. Journal of Fluid Mechanics 503, 357–374.

Steward, D.R., 2002. A vector potential and exact flux through surfaces using Lagrange and Stokes stream functions. Source: Proceedings Royal Society London A 458, 489–509.

Steward, D.R., Jin, W., 2001. Gaining and losing sections of horizontal wells. Water Resources Research 37, 2677–2685.

Strack, O.D.L., 2003. Theory and applications of the analytic element method. Review of Geophysics 41 (art. no. 1005).

Warrick, A.W., Fennemore, G.G., 1995. Unsaturated water flow around obstructions simulated by two-dimensional Rankine bodies. Advances in Water Research 18 (6), 375–385.

Wolfram, S., 1991. Mathematica. A System for Doing Mathematics by Computer. Addison-Wesley, Redwood City.

Yechieli, Y., Wood, W.W., 2002. Hydrogeologic processes in saline systems: playas, sabkhas, and saline lakes. Earth-Science Review 58, 343–365.